Received Date : 05-Nov-2013
Revised Date : 21-Feb-2014
Accepted Date : 17-Mar-2014
Article type : Original Article

Manuscript Category: Signaling & Cell biology (SCB)

# Melanosome-autonomous regulation of size and number:

# The oa1 receptor sustains pmel expression

Paola Falletta[1], Paola Bagnato[1], Maria Bono[1], Massimiliano Monticone[2],

Maria Vittoria Schiaffino[3], Dorothy C. Bennett[4], Colin R. Goding[5],

Carlo Tacchetti[1,6] and Caterina Valetti[1]

[1] Department of Experimental Medicine, University of Genoa, 16132, Genoa, Italy

[2]RCCS Azienda Ospedaliera Universitaria San Martino - IST - Istituto Nazionale per la Ricerca sul Cancro, Genoa, Italy

[3]San Raffaele Scientific Institute, Center for Translational Genomics and Bioinformatics, Milan, Italy

[4]Division of Biomedical Sciences, St. George's, University of London, Cranmer Terrace, London, UK

[5]Ludwig Institute for Cancer Research, Nuffield Department of Clinical Medicine, University of Oxford, Headington, Oxford, UK

[6]San Raffaele Scientific Institute, Experimental Imaging Center, Milan, Italy

*Running title: OA1 regulation of MITF in melanosome biogenesis*

Corresponding authors: Caterina Valetti: valetti@unige.it; Carlo Tacchetti: carlo.tacchetti@unige.it

SUMMARY

Little is known as to how cells ensure that organelle size and number are coordinated to correctly couple organelle biogenesis to the demands of proliferation or differentiation. OA1 is a melanosome-associated G-protein-coupled receptor involved in melanosome biogenesis during melanocyte differentiation. Cells lacking OA1 contain fewer, but larger, mature melanosomes. Here we show that

This article has been accepted for publication and undergone full peer review but has not been through the copyediting, typesetting, pagination and proofreading process, which may lead to differences between this version and the Version of Record. Please cite this article as doi: 10.1111/pcmr.12239

OA1 loss-of-function reduces both the basal expression and the αMSH/cAMP-dependent induction of the microphthalmia-associated transcription factor (MITF), the master regulator of melanocyte differentiation. In turn, this leads to a significant reduction in expression of PMEL, a major melanosomal structural protein, but does not affect tyrosinase and melanin levels. In line with its pivotal role in sensing melanosome maturation, OA1 expression rescues melanosome biogenesis, activates MITF expression and thereby coordinates melanosome size and number, providing a quality-control mechanism for the organelle in which resides. Thus, resident sensor receptors can activate a transcriptional cascade to specifically promote organelle biogenesis.

SIGNIFICANCE

The melanosome is an excellent model to study the mechanisms regulating organelle biogenesis. Fewer, but bigger melanosomes (macromelanosomes) are observed in cells deficient in OA1, a melanosomal resident G-protein coupled receptor. Here we show that OA1 regulates melanosome size and number via activation of the Microphthalmia-associated transcription factor, the "master regulator" of melanocyte differentiation. These observations suggest a general mechanism for regulation of organelle biogenesis in which organelle-specific proteins act as both sensors and modulators of maturation state.

INTRODUCTION

Organelle biogenesis is a complex process highlighted by the timed synthesis and sorting of specific structural and functional proteins. How these events are regulated to modulate the rate of production and size of the organelles is an intriguing issue in cell biology. Melanosome biogenesis can serve as a model system to unravel some of these processes. Melanosomes are distinctive pigmented organelles of skin melanocytes, the Retinal Pigment Epithelium (RPE) and the choroid, and represent the primary site of melanin synthesis and storage. Although characterized by the expression of a set of proteins conferring morphological and functional specificity, they are classified as Lysosome-Related Organelles (LROs), as they segregate from the conventional endocytic pathway, and express some of the late endosome and lysosome markers (Marks et al., 2013).

Based on morphology, melanosomes can be classified into four ultrastructurally and biochemically distinct stages (Marks & Seabra, 2001): *Stage I*, corresponding to coated endosomes (Berson et al, 2001; Theos et al, 2006b), that is the vacuolar domain of early endosomes; *Stage II* are elliptical unpigmented organelles containing a well-organized fibrillar matrix; *Stage III and IV* are marked by the presence of melanin deposited along the fibrils in stage III, which at stage IV completely fills the lumen of the organelle. The key enzyme involved in the synthesis of melanin from the initial precursor tyrosine is Tyrosinase (TYR). Premelanosome protein (PMEL also known as PMEL17, SILV or gp100) is an integral membrane glycoprotein that segregates with coated endosomes and undergoes several steps of cleavage and maturation (Hurbain et al, 2008) to constitute

the major component of the melanosome fibrillar matrix observed in stage II and III melanosomes (Berson et al, 2003; Kobayashi et al, 1994; Theos et al, 2006a). The PMEL fibrillar matrix serves as a scaffold to focus melanin polymerization (McGlinchey et al, 2009), and to sequester toxic melanin biosynthesis intermediates in later stage melanosomes (Watt et al, 2009). The key role of PMEL in melanosome maturation is highlighted in animal models carrying *Pmel* mutations that show varying levels of hypopigmentation, from mild to severe (Watt et al, 2011). For example, in the *silver* (*Pmel*) mutant (hPmel17si) mouse model (Theos et al, 2006a), PMEL is inefficiently exported from the endoplasmic reticulum and its accumulation within pre-melanosomes is significantly decreased. As a consequence, melanosomes from *silver* mice display reduced striations and an aberrant enlarged 'giant' spherical shape. Notably these melanosomes are densely pigmented (Solano et al, 2000; Theos et al, 2006b).

The rate of maturation and size of melanosomes are finely tuned, and aberrant melanosome size is a hallmark of several genetic disorders characterized by organelle biogenesis defects. For example, both Chediak-Higashi and Hermansky–Pudlak syndromes display enlarged melanosomes (macromelanosomes) owing to aberrant fusion of pre-existing organelles (Introne et al, 1999). By contrast, the macromelanosomes found in the RPE and skin melanocytes from Ocular Albinism type 1 (OA1) patients and *Oa1* knock-out (melan-$Oa1^{-/-}$) mice, originate from the overgrowth of single melanosomes (Incerti et al, 2000; Palmisano et al, 2008). In this disease, melanosomes display a single melanin-coated fibrillar matrix core, similar in size and structure to that of a normal melanosome, and exhibit no intermediates of melanosome-melanosome fusion (Incerti et al, 2000) Beside melanosome enlargement, Ocular Albinism type 1 patients display a severe reduction in the number of stage II melanosomes (Schiaffino et al, 2002). The phenotype is even more dramatic in RPE cells of fetal and adult patients (O'Donnell et al, 1976). When analyzed in *Oa1* knock-out (melan-$Oa1^{-/-}$) mice, macromelanosomes appear to increase progressively in size and number from embryo to adulthood, when the majority of melanosomes display the giant phenotype, and the number of mature melanosomes is reduced by 50% (Cortese et al, 2005).

OA1 is an atypical G-protein-coupled receptor (GPCR) (Innamorati et al, 2006; Schiaffino et al, 1999; Staleva & Orlow, 2006) as unlike other GPCRs, it is primarily associated with intracellular endo-lysosomes and melanosomes, with its N-terminus located towards the lumen of the organelle and its C-terminus towards the cytoplasm (Chi et al, 2006; Giordano et al, 2009; Samaraweera et al, 2001). Collectively, these observations suggest that OA1 may provide the cell with a mechanism to sense melanosome maturation and regulate organelle biogenesis and homeostasis. However, while the first component of the signaling cascade triggered by OA1 has been identified in Gαi3 (Young et al, 2011), the identity of its downstream targets and cause of macromelanosome production remain unknown.

Here we demonstrate that the organelle receptor OA1 acts as a biosensor to modulate the rate of organelle production, by regulating the expression of the transcription factor MITF, the master regulator of melanocyte development, function, survival and cell-cycle progression (Vachtenheim &

Borovansky, 2010). In the absence of OA1, a decrease in MITF levels leads to a diminished transcription of melanosome biogenesis genes, affecting primarily PMEL protein levels, with a minimal effect on the rate of melanin biosynthesis. Since the reduced amount of PMEL is responsible for the onset of enlarged melanosomes in the hPmel17si cell line, we conclude that the diminished PMEL causes the enlarged melanosomes formation observed in *Oa1* mutant cells.

RESULTS

**_Oa1_-KO melanocytes display melanosome rate of maturation and size defects**

Ocular Albinism type 1 patients are characterized by a reduced number of mature melanosomes that exhibit increased size in both skin melanocytes and in RPE cells (Garner & Jay, 1980; O'Donnell et al, 1976) Mouse $Oa1^{-/-}$ melanocyte cells (Palmisano et al, 2008) show a similar phenotype and can be considered a bona fide *in vitro* cell model of OA1 loss-of-function melanocytes.

Compared to *wild-type* mouse melanocytes melan-A ($Oa1^{+/+}$) (Figure 1A, A'), $Oa1^{-/-}$ cells are characterized by different distribution of the pigmented melanosomes (Figure 1B) and frequently by the presence of long and branched dendrites (Figure 1B'). In particular, in comparison to $Oa1^{+/+}$ cells, pigmented melanosomes in $Oa1^{-/-}$ cells are sparsely distributed in the central area, and concentrated at the cell periphery and in the long dendrites (Figure 1A, B). These observations are in line with the data obtained by Palmisano et al., 2008, in which OA1 has been demonstrated to control melanosome distribution regulating microtubule-mediated motility. Of note, we further evaluated the role of the actin cytoskeleton and Rab27a, a component of the Rab27a-melanophilin (Slac2a-Mlph) complex, that controls melanocyte dendriticity and melanosome transport (Chiaverini et al., 2008), allowing melanosomes to move on the actin network, and found that they are not affected by the presence of OA1 (Figure S1). Both microscopic (Figure 1A, B) and ultrastructural analysis using a flat-embedding technique to preserve the original shape and organelle distribution in cultured cells (Figure 1C, D), show an even distribution of unpigmented/low-pigmented stage II/III melanosomes in the central and peripheral area in $Oa1^{+/+}$ cells, but an absence from the central area in $Oa1^{-/-}$ cells. Quantification of melanosome number coupled with a morphometric analysis shows that the number of stage II, III and IV melanosomes is 20, 5, and 2-fold reduced in $Oa1^{-/-}$ cells, compared to $Oa1^{+/+}$ cells, respectively (Figure 1E). Moreover, mature melanosomes in $Oa1^{-/-}$ cells are on average larger compared to *wild-type* cells (Figure 1F). Indeed, over 60% of the stage IV melanosomes can be classified as 'ENLARGED' (diameter range 0.6µm - 0.9µm), and 'MACRO' (diameter > 0.9µm), and only about 40% display the normal size (diameter <0.6µm). Notwithstanding the changes in number and size of melanosomes, $Oa1^{-/-}$ and $Oa1^{+/+}$ cells contain comparable amounts of melanin (Figure 1G), suggesting that the reduced number of stage IV melanosomes is counterbalanced by a higher content of melanin per melanosome, due to the increased size.

These results suggest that OA1 may be part of a mechanism that modulates the rate of *de novo* melanosome biogenesis, rather than the expression of components of the enzymatic cascade responsible for melanin biosynthesis.

**OA1 re-expression in *Oa1*$^{-/-}$ cells rescues number and size of melanosomes**

A functional role for OA1 in melanosome biogenesis implies that OA1 re-expression in *Oa1*$^{-/-}$ cells should provide a phenotypic rescue and restore the amount of early stage melanosomes and reduce the size of the macromelanosomes. We therefore stably transduced *Oa1*$^{-/-}$ melanocytes with retroviral vectors carrying the *wild-type Oa1* (L*Oa1*SN), or an empty vector as control (LSN). By immunofluorescence, the resulting *Oa1*$^{-/-}$L*Oa1*SN melanocytes show stable OA1 expression in about 50% of the cells, with OA1 displaying the expected intracellular distribution in endo-lyso-melanosomal compartments (Figure 2A) (Giordano et al, 2009; Schiaffino et al, 1999; Shen et al, 2001).

EM analysis by flat embedding reveals that, compared to control *Oa1*$^{-/-}$ LSN cells (Figure 2B), OA1 rescue in *Oa1*$^{-/-}$L*Oa1*SN (Figure 2C) leads to a significant increase in the total number of stage II melanosomes. Quantification demonstrates that although we find no significant variation in the total number of stage III and IV melanosomes (Figure 2D), the melanosomes in cells re-expressing OA1 are mostly localized in the central area, leading to a significant difference between the *Oa1*$^{-/-}$ LSN cells and those re-expressing OA1 (Figure 2E), while in the dendritic area the amount of melanosomes of all stages is not affected by OA1 re-expression (Figure 2F). Furthermore, we observe a pronounced reduction of stage IV 'ENLARGED' (diameter: 0.6-0.9 μm) and 'MACRO' (diameter: >0.9 μm) melanosomes, and a sensitive increase in the number of normal (diameter: 0.2-0.6 μm) stage IV melanosomes (Figure 2G).

These data demonstrate that OA1 restoration rescues the *OA1*$^{-/-}$ phenotype, leading to an increase in number of early stage melanosomes, and a decrease in size of mature melanosomes, and confirms that the primary defect in these cells arises from mutation of the *Oa1* gene.

**OA1 controls melanosome structural protein expression but not melanin biogenesis**

Our data indicate that OA1 may play a role in regulating the rate of early melanosome biogenesis, possibly by regulating the expression of early melanosome structural components. To verify this hypothesis we measured the level of PMEL and TYR. PMEL is a structural component of melanosomes that participates in the organization of the melanosome matrix fibrillar scaffold, and a series of cleavage and maturation steps of PMEL generates the P1 and Mβ forms that characterize the progression from stage I to stage II melanosomes (Berson et al, 2001). By contrast the activity of TYR, the first rate-limiting enzyme of the melanin biosynthetic pathway, determines the morphological transition from unpigmented stage II, to pigmented stage III and IV melanosomes.

When analyzed by Western Blot, the expression of both the processed forms P1 and Mβ of PMEL positively correlate with the expression of OA1, with reduced expression observed in *Oa1*$^{-/-}$ compared to *Oa1*$^{+/+}$ melanocytes (Figure 3A). The housekeeping protein Calnexin (CLN) is used as a loading control. Consistent with this, stable shRNA-mediated inactivation of OA1 (Figure S2) in

*Oa1*$^{+/-}$ cells (shOA1) leads to a similar reduction in the expression of the processed forms of PMEL (Figure 3A and B). By contrast, the levels of TYR protein are unaffected in both *Oa1*$^{-/-}$ and shOA1 cells (Figure 3A and B). However, when we analyzed the *Pmel* and *Tyr* mRNA levels in *Oa1*$^{-/-}$ and *Oa1*$^{+/+}$ melanocytes (Figure 3C), we found that both are reduced. Therefore, although OA1 appears to modulate the transcription of both the *Pmel* and *Tyr* genes, its effect appears to be restricted to PMEL protein expression. These results may be partially explained by the long TYR protein half-life (Saeki & Oikawa, 1980), such that a low amount of *Tyr* mRNA in *Oa1*$^{-/-}$ cells is sufficient to maintain a sizable amount of TYR enzyme and consequently a similar amount of melanin to that observed in wild type cells. Collectively these data suggest a previously unidentified role for OA1 in the regulation of the expression of genes involved in melanosome biogenesis.

**OA1 sustains MITF expression in melanocytes**

Our observations suggest that OA1 may be involved in the modulation of the early stages of melanosome maturation. Therefore, we sought a possible connection between the expression of OA1 and MITF that coordinates the expression of genes implicated in melanin synthesis and melanosome biogenesis and transport, including *Pmel* (Du et al, 2003) and *Tyr* (Bentley et al, 1994; Du et al, 2003). When comparing wild type Melan-a melanocytes (derived from the skin of C57BL/6J mice), to wild type *Oa1*$^{+/+}$, and *Oa1*$^{+/-}$ versus *Oa1*$^{-/-}$ melanocytes (the latter three derived from 129/Sv mice) (Palmisano et al, 2008), we observed a dramatic decrease in MITF protein levels (Figure 4A, left panel) when OA1 expression is absent. The requirement for OA1 in MITF expression was confirmed using cells depleted for OA1 using shRNA (Figure 4A, right panel). The reduced MITF expression in *Oa1*$^{-/-}$ or shRNA-depleted melanocytes found using western blotting was also observed by immunofluorescence with a lower MITF nuclear staining seen in cells with reduced OA1 expression (Figure 4B).

The positive regulation of MITF expression by OA1 may occur through two non-exclusive mechanisms: inhibition of MITF protein degradation (post-translational regulation), and/or a positive control on transcription of the MITF gene. The analysis of MITF protein half-life in *Oa1*$^{+/+}$ and *Oa1*$^{-/-}$ cells using cycloheximide (CHX) as a protein synthesis inhibitor revealed an almost identical degradation kinetic (Figure 4C, left panel). Similar observations were made when comparing shCTR and shOA1 cells (Figure 4C, right panel). By contrast, the analysis of *Mitf* mRNA levels (Figure 4D) revealed a sizable decrease in both *Oa1*$^{-/-}$ (45%) and shOA1 (55%) cells, compared to *Oa1*$^{+/+}$ and shCTR, respectively. Thus, it appears that the reduced MITF protein seen in OA1-negative cells correlates with decreased *Mitf* mRNA expression, suggesting that at least at steady state, post-translational regulation mechanisms are unlikely to be involved in the down-regulation of MITF expression. These results therefore define OA1 as a signaling protein controlling *Mitf* mRNA levels.

To further substantiate this model, we examined MITF expression in the *Oa1*$^{-/-}$ cells in which

retroviral infection was used to re-express OA1 and restore normal melanosome morphology (Figure 2). The results (Figure 5A) confirmed that OA1 regulates MITF expression. Thus, while the control *Oa1*$^{-/-}$ melanocytes (LSN) exhibit low levels of MITF, re-expression of OA1 in the *Oa1*$^{-/-}$L*Oa1*SN melanocyte cell line restored MITF protein levels. Consistent with this, western blot analysis reveals a rescue in the amount of both P and Mβ processed forms of PMEL in *Oa1*$^{-/-}$L*Oa1*SN, compared to control, confirming that OA1 regulates PMEL protein levels (Figure 5B). The restoration of PMEL expression is likely mediated by MITF, as MITF re-expression in *Oa1*$^{-/-}$ cells shows an increase of both P and Mβ processed forms of PMEL (Figure 5C). The increase in PMEL protein detected by western blotting in *Oa1*$^{-/-}$L*Oa1*SN melanocytes compared to control was paralleled by an increased number of PMEL-positive organelles in the central area (Figure 5D and Figure S3). These organelles can be identified as early stage melanosomes using the HMB45 anti-PMEL antibody, to detect fragments of PMEL detectable only in stage II melanosomes (FIGURE). Taken together these data suggest that OA1 regulates PMEL expression via MITF.

Because both the *Pmel* and *Tyr* genes are under the control of MITF, but only PMEL appears to be affected by its modulation via OA1, we asked whether other MITF controlled genes could have a similar behaviour. In particular, we studied MART1, an MITF target (Du et al., 2003) and escort protein for OA1 (Giordano et al., 2009), and found (Figure S3) that, similarly to Rab27a (Fig. S2) and tyrosinase (Fig. 3), the presence of OA1 affects neither the amount nor the distribution of the MART1 protein. This observations leads to the hypothesis that the reduced amount of MITF in OA1 depleted cells results in a selective down-regulation of PMEL protein, leaving unaffected other MITF target genes. A possible explanation could be that a secondary level of regulation MITF-dependent, acting at post-translational level, can specifically affect PMEL protein stability.

### *Oa1*$^{-/-}$ melanocytes exhibit a defective response to αMSH

If OA1 positively controls MITF, which in turn regulates the expression of *Pmel* and *Tyr,* major genes involved in the biogenesis of melanosomes, in the absence of OA1 the signaling pathways upstream of *Mitf* should be impaired. In skin melanocytes, the growth factor αmelanocyte-stimulating hormone (αMSH) is a key regulator of melanosome biogenesis and melanin synthesis. αMSH binding to its GPCR, the melanocortin 1 receptor, induces MITF expression via cAMP-driven phosphorylation and activation of cAMP-response element binding protein CREB that recognizes the *Mitf* promoter (Bertolotto et al, 1998). To verify the physiological role of OA1 in regulating MITF, we asked whether OA1 is involved in the αMSH-*Mitf* signaling cascade. We first stimulated wild type and *Oa1*$^{-/-}$ melanocytes with αMSH and examined MITF protein expression over time. In wild type melanocytes (Figure 6A, upper panel) αMSH leads to a sustained elevation in MITF expression that continues for at least 24 h. By contrast, *Oa1*$^{-/-}$ melanocytes (Figure 6A, lower panel) exhibit a similar initial stimulation of MITF expression, but by 6h MITF expression had returned to almost basal levels. To

be noted: in this kinetics, double amount of cell extracts have been loaded for OA1 deficient melanocytes, compared to control cells, to better visualize and quantify band intensity. Quantification of these data is shown in Figure 6B. The striking difference in kinetic of MITF expression between OA1 wild type and *Oa1*$^{-/-}$ melanocytes in response to αMSH treatment was reproduced when comparing control and OA1-specific shRNA expressing cells (Figure 6C). We obtained similar results when stimulating the cells with the cAMP agonist forskolin (not shown), which mimics αMSH signaling (Price et al, 1998). Collectively these results indicate that, although cells depleted for OA1 are able to respond to an αMSH stimulus, they are unable to sustain the response, reinforcing the observation that OA1 plays a role in αMSH-induced regulation of MITF.

As we excluded a role for OA1 as negative modulator of the efficiency of MITF protein degradation (see Figure 4C), we sought to confirm this observation in αMSH-stimulated cells. Accordingly, we treated *Oa1*$^{+/+}$ and *Oa1*$^{-/-}$ cells with αMSH and, after 3h of treatment, corresponding to the major peak of MITF expression, added the protein synthesis inhibitor CHX) (Figure 6D). While *Oa1*$^{+/+}$ melanocytes respond to CHX treatment with a rapid decrease of MITF protein levels compared to cells not exposed to CHX, *Oa1*$^{-/-}$ cells display a rapid decrease in MITF protein in both CHX treated and untreated conditions. These data allow us to exclude a possible role for OA1 in inhibition of MITF protein degradation, and to assign the primary role of OA1 in regulating the *Mitf* mRNA expression.

The results obtained from measuring MITF protein expression in response to αMSH were reflected in *Mitf* mRNA levels. In the presence of OA1 we observed a progressive increase in *Mitf* mRNA levels on αMSH treatment. By contrast, in *Oa1*$^{-/-}$ melanocytes we observed a peak of *Mitf* mRNA after 1h of αMSH treatment, followed by a rapid decrease between 1h and 3h that drops below the initial basal level (Figure 7A).

mRNA transcription and degradation rates are coordinately regulated to allow temporal modulation of gene expression (Proudfoot et al, 2002). The analysis of the 3'UTR of the *Mitf* mRNA reveals potential mRNA instability elements, such as the adenylate/uridylate-rich element (ARE) (Haflidadottir et al, 2010), suggesting that *Mitf* mRNA may be susceptible to a rapid degradation. Therefore, we asked whether OA1 activity could lead to a reduced *Mitf* mRNA degradation by analyzing the half-life of *Mitf* mRNA using Actinomycin D (ActD) as a transcriptional inhibitor. The results revealed that ActD administration to cells stimulated with αMSH for 2h, corresponding to the major peak of *Mitf* expression, induced *Oa1*$^{+/+}$ melanocytes to respond with a decrease in *Mitf* mRNA levels compared to untreated control cells (Figure 7B). By contrast, in *Oa1*$^{-/-}$ cells ActD treatment does not induce any substantial change in the profile of *Mitf* mRNA levels following αMSH treatment (Figure 7C).

Finally, ActD treatment of *Oa1*$^{+/+}$ and *Oa1*$^{-/-}$ cells at steady state in the absence of αMSH stimulus (Figure 7D) reveals a differential effect in the two cell lines. In the control *Oa1*$^{+/+}$ cells, *Mitf* mRNA is rapidly degraded with a half-life of approximately 90 min. This finding confirms that *Mitf*

mRNA is an unstable and presumably highly regulated mRNA. Surprisingly, however, in *Oa1*$^{-/-}$ cells, where the basal level of MITF expression is low, we do not observe any evidence for *Mitf* mRNA degradation on ActD treatment (Figure 7D). Indeed the level of *Mitf* mRNA achieved after prolonged ActD treatment of *Oa1*$^{+/+}$ cells appears to be similar to the basal level exhibited by *Oa1*$^{-/-}$ cells. This observation raises the possibility that the fraction of *Mitf* mRNA in wild type cells that is stable and persists after ActD treatment, is similar to that expressed at the steady state in the *Oa1*$^{-/-}$ cells. Thus there may be a minimum threshold below which the *Mitf* mRNA degradation is impaired (Figure 7D). Collectively these data support the notion that one role for OA1 is the control of de novo melanosome biogenesis via regulation of *Mitf* mRNA expression.

## DISCUSSION

Melanosome maturation relies on the combined role of structural proteins (e.g. PMEL), and enzymes involved in melanin synthesis. The two sets of proteins need to be coordinately regulated, so that melanin synthesis can occur when the melanosome has assembled the proper fibrillar scaffold (stage II melanosomes), and terminate when full maturation of melanosomes is reached (stage IV melanosomes). Several aspects of this process are still unclear. For example, how the structural events leading to the onset of a new melanosome biogenesis (ultimately controlling the density of melanosomes in a given melanocyte) are linked to the regulation of the expression of enzymes involved in melanin biosynthesis, and which mechanisms control the size of a melanosome.

A pivotal role in the regulation of melanosome biogenesis is played by the protein OA1, a GPCR that has an unusual and exclusive localization to intracellular endo-lyso-melanosomal membranes (Schiaffino, 2010). OA1 loss-of-function leads to a reduction in number of early stage melanosomes, and the presence of macromelanosomes (Cortese et al, 2005; Schiaffino, 2010; Schiaffino et al, 2002). However, although melanosome biogenesis and melanin synthesis are generally considered linked, we show here that the reduction of melanosome number in *Oa1*$^{-/-}$ cells is not associated with reduced melanin content. A possible explanation for this observation is that most likely the reduced number of melanosomes in OA1-negative cells is compensated by the increased size of stage IV highly pigmented melanosomes. These data support the observation that levels of TYR expression (Vetrini et al, 2006), and activity (Cortese et al, 2005), as well as expression of TYRP1, another pigmentation enzyme (Giordano et al, 2009), are not affected by OA1 loss-of function. This is in line with the knowledge that the formation of macromelanosomes in *Oa1*$^{-/-}$ cells is due to the overgrowth of single melanosomes rather than by the fusion of existing melanosomes (Incerti et al, 2000).

We also underline that stage II melanosomes observed in *Oa1*$^{-/-}$ cells display normal size and morphology as occurs in RPE from KO mice (Cortese et al, 2005), suggesting that the ability to synthesize melanin to normal levels, and the reduced rate of organelle biogenesis, are both necessary for macromelanosome formation. The biogenesis of macromelanosomes, in view of the unimpaired

efficiency in melanin synthesis observed in *Oa1*$^{-/-}$ cells, may therefore be explained by a model in which each of the few newly formed melanosomes receives a higher ratio of melanin synthesis-enzymes, leading to an increase in the relative content of pigment (Figure 8). However, if this model is correct, it should also include a mechanism to bypass a putative 'size vs maturation control' operated at the level of the single melanosome by a possible 'biosensor'. Alternatively, one could imagine the presence of a 'biosensor', signaling from pigmented melanosomes, regulating the rate of new melanosome biogenesis.

We hypothesize that OA1 may represent the putative candidate for both types of 'biosensor'. OA1 could be a melanin synthesis biosensor, signaling from late stage (III and IV) pigmented melanosomes, to promote new melanosome biogenesis. That signaling by OA1 might be restricted to later stages of melanosome maturation would also be consistent with the normal stage II melanosomes observed in *Oa1*$^{-/-}$ cells.

In support of this hypothesis, we show in this study that OA1 activity leads to the regulation of *Mitf,* the key gene involved in melanogenesis. MITF is a transcription factor known to regulate the expression of both melanosome scaffold proteins and enzymes involved in melanin synthesis. Our data show that in the absence of OA1 there is a dramatic reduction of MITF, although to levels still sufficient to sustain the survival and differentiated status of the pigmented cell (Steingrímsson et al, 2004). However, the reduced level of MITF leads to a selective reduced expression of the structural protein PMEL, and not of TYR, the key enzyme necessary for melanin synthesis, and of other MITF target genes, i.e. MART1 and Rab27a. These data explain why lack of OA1 correlates with a reduced number of newly formed melanosomes, but normal melanin levels. Therefore we propose a model where a decrease in PMEL expression is responsible for a reduced rate of new stage II melanosome formation, rather than impairing the formation of correctly assembled fibrillar structures of a single melanosome (Figure 8). The normal rate of melanin synthesis enzyme expression (e.g. tyrosinase), will eventually lead to relative increase of these enzymes for each residual stage II melanosomes, the synthesis of an excess of melanin per melanosome and the formation of macromelanosomes (Figure 8).

In support of this model, OA1 re-expression, enables the recovery of *Mitf* transcription, leading to a high MITF expression, and correlates with a re-activation of stage II melanosome biogenesis.

Quite surprisingly, however, we also observe that MITF overexpression in *Oa1*$^{-/-}$, although leading to a sizable increase of PMEL protein levels, does not lead to an increase in melanosome biogenesis. This observation indicates that MITF is necessary but not sufficient for the onset of melanosome biogenesis, and additional factors are necessary for melanosome formation. A fascinating hypothesis could be that OA1 is able to regulate other structural components of the melanosome, such as membrane amount and composition. Another explanation for the lack of melanosome biogenesis upon MITF overexpression is that the MITF protein levels or post-translational modifications differ from the physiological levels present in wild type cells, affecting

MITF activity and affinity for its target genes.

Our data are in line with the concept that MITF activity and expression can be finely tuned in pigmented cells, to contribute to the homeostasis of several cell processes. In melanoma for instance, MITF, rather than working as a simple on/off switch, appears to act as a rheostat integrating a wide variety of signaling events regulating its expression and activity (Carreira et al, 2005). Similarly, in OA1 loss-of-function cells, MITF may be finely tuned and regulated in order to maintain the basic functions related to cell survival. Of interest, at steady state we noticed a negligible *Mitf* mRNA turnover in *Oa1* knock-out cells, compared to *wild-type* melanocytes, suggesting that at the low basal levels of *Mitf* mRNA observed in *Oa1*$^{-/-}$ cells, a critical concentration is reached at which the *Mitf* mRNA degradation is likely impaired. This observation leads to the hypothesis that in the absence of OA1 signaling, despite a reduction of *Mitf* transcriptional activation, compensative mechanisms may be switched on, to counterbalance the lack of MITF, allowing maintenance of homeostasis in the cell.

To define the signaling pathway by which OA1 regulates *Mitf* expression, we analyzed the major signaling pathway leading to *Mitf* expression upon αMSH stimulation, i.e. the αMSH-cAMP-CREB pathway (Price et al, 1998). αMSH leads to a rapid increase in MITF expression and activation, and to the production of melanin coupled with melanosome biogenesis. Our data indicate that OA1 participates in this pathway and is necessary to maintain an appropriate level of *Mitf* mRNA and protein since in the absence of OA1, αMSH triggers only a transient activation of MITF expression.

Taken together our data indicate that melanosomes require OA1 to modulate their own maturation and the rate of new melanosome formation. The downstream signaling involves the control of the master regulator of the pigmented cell MITF expression. A similar mechanism of autonomous regulation has been demonstrated recently for lysosome biogenesis: lysosomes sense their content and regulate their own biogenesis by a lysosome-to-nucleus signalling mechanism involving the MITF-related transcription factor TFEB and mTOR (Settembre et al, 2012), although TFEB activation is mediated by post-translational modification and not through gene transcription. Our results suggest that a similar mechanism occurs for melanosome-autonomous regulation of number, size and composition, via OA1 that acts as specialized regulator in the wider process that takes place in the cell to control the biogenesis of the organelle.

## MATERIALS AND METHODS

### Reagents

αMSH, Forskolin and ActD were from Sigma-Aldrich, and CHX from Calbiochem.

### Cell culture

*Oa1*$^{+/+}$ (melan-*Oa1*$^{+/+}$ cells, also known as melan-A cells from their *A/A* agouti phenotype), *Oa1*$^{+/-}$ (melan-*Oa1*$^{+/-}$ cells) and *Oa1*$^{-/-}$ (melan-*Oa1*$^{-/-}$ cells) were established from female agouti 129/Sv mice

(Incerti et al, 2000). Melan-a cells were described by Bennett et al, 1987.

Cell culture conditions are carefully described at the web page Wellcome Trust Functional Genomics Cell Bank (http://www.sgul.ac.uk/depts/anatomy/pages/dcbhmpg.htm) and in Palmisano et al, 2008. These cell lines may show spontaneous depigmentation: particular attention has been paid to not use cells undergoing spontaneous depigmentation.

***Oa1* Silencing by RNA interference**

*Oa1* silencing of *Oa1*$^{+/-}$ cells was obtained by vector-driven expression of sequence-specific shRNAs (Paddison et al., 2002). A pcDNA4TO (Invitrogen)-based shRNA expression vector was derived from the previously described pTER (van de Wetering et al, 2003) by inserting the CMV enhancer upstream of the H1 promoter, driving the expression of a shRNA cassette (pCMVTER vector). Four putative 21 bp target sequences in the *Oa1* cDNA (accession number X98352) were identified using the SFOLD on-line application (http://sfold.wadsworth.org/sirna.pl). Complementary 63 bp oligonucleotide pairs, designed to generate sticky ends complementary to BglII/HindIII sites and a shRNA cassette specific for the target sequences upon annealing, were generated and cloned into pCMVTER. In preliminary experiments, only one target sequence, shOA1, showed the ability to efficiently downregulate co-expressed *Oa1*, while other shRNAs gave minimal effects (not shown). *Oa1*+/- subclone #5 melanocytes (see Palmisano et al, 2008) were transfected with pCMVTER plasmids in 6 cm plates: pCMVTER either empty (shCTR), carrying ineffective shSCR or specific shOA1. Seventy-two hours post-transfection, melanocytes were transferred to 10 cm plates and selected with 400 μg/ml zeocin (Invitrogen), which was maintained thereafter in order to avoid loss of plasmid integration. Complementary 63 bp oligonucleotides for shOA1 (target sequence in *Oa1* cDNA: 695-713) and shSCR were as follows (underlined are the cloning sites; in bold are the sense and antisense target sequences; in italic are some C to T substitutions in the sense strand, to reduce the incidence of mutations in bacteria due to "cross formation" during DNA replication):

shOA1

5'GATCC**AAC*T*CAAT*T*CTGTTACACA**TTCAAGAGA**TGTGTAACAGGATTGGGTT**TTTTTT TGGAAA

5'AGCTTTTCCAAAAAA**AACCCAATCCTGTTACACA**TCTCTTGAA**TGTGTAACAG*A*ATT G*A*GTT**G

The quality of *Oa1* silencing was determined by semi-quantitative PCR: cytoplasmic RNA was isolated with RNeasy Mini kit (Qiagen), and reverse transcribed with oligo(dT) primers using the SuperScript First-Strand Synthesis System for RT-PCR kit (Invitrogen), according to manufacturers' instructions. Semi-quantitative PCR reactions were carried out in a total volume of 100 μl using Taq polymerase (Promega) and 1 μl of cDNA as template. β-actin was used to normalize the cDNA

concentrations and amplified by using primers β-actin F:5'-GGCATCGTGATGGACTCCG and β-actin R: 5'-GCTGGAAGGTGGACAGCGA. *Oa1* was amplified by using primers FmOA1(1064): 5'-AATGACTGCCTCTGCTGCTGA and RmOA1(1552): 5'-ATGGATTTGGATCTGGCACTT.
Semi-quantitative PCR conditions were 1 cycle at 95°C for 5min, 30 cycles at 95°C for 30 sec, 55°C (β-actin) or 57°C (*Oa1*) for 30 sec, 72°C for 1min, and 1 cycle at 72°C for 5 min. During the amplifications, which were performed simultaneously for the different cell lines, 20 µl were collected at cycles 16/18/20/22 from the β-actin reactions and at cycles 18/20/22/24 from the *Oa1* reactions. The semi-quantitative PCR is shown in Figure S2.

**Expression vectors and retroviral infection**

The L*Oa1*SN retroviral vector, carrying the *Oa1* cDNA, was a generous gift from Valeria Marigo (University of Modena and Reggio Emilia, Italy), and was obtained by cloning the *Oa1* cDNA into the *Eco*RI and *Xho*I sites of the LXSN retroviral vector (Miller & Rosman, 1989). The pBabe-*Mitf* retroviral vector was constructed by cloning a full length Bgl-2 fragment of the *Mitf* cDNA into the BamHI site of pBabe (Morgenstern & Land, 1990). Throughout this paper *Mitf* refers to the *Mitf*-M(+) isoform and the cDNA used was of mouse origin. The *eco*-tropic packaging cell line Phoenix was transfected by the calcium-phosphate/chloroquine method. Twenty-four hours after transfection, the medium was changed, and culture supernatants containing viral particles were collected after additional 24h and 48h. The retroviral supernatant was supplemented with polybrene (Sigma) at 5 µg/ml and used for melanocyte infection. Two infection cycles lasting 3h and spaced out by 24h were performed to infect $Oa1^{-/-}$ cells.
Forty-four hours post infection, cells were selected as a polyclonal population with 750 µg/ml of G418 (Sigma), which was maintained thereafter in order to avoid loss of retroviral integration (Kinsella & Nolan, 1996).
The cell lines obtained were designated $Oa1^{-/-}$L*Oa1*SN, $Oa1^{-/-}$LSN and pBabe, pBabe-*Mitf*

**Cell lysis, immunoblotting and quantification**

Cells were lysed in RIPA lysis buffer [Triton-X100 1%, Na deoxycholate 1%, SDS 0.1%, NaCl 150 mM, Tris HCl 50 mM] for nuclear proteins and in Nonidet P40 buffer [NP40 1%, EDTA 5 mM, NaCl 150 mM, Tris pH 7.5 l50 mM] for melanosomal proteins, both supplemented with a complete protease inhibitor cocktail (Roche). Protein concentration was determined by Bio-Rad Protein Assay (BioRad) and equal amounts of proteins (20-60µg) were loaded and separated in 7.5% SDS-PAGE for nuclear proteins and 10% for melanosomal proteins. The separated proteins were then transferred to nitrocellulose membranes, probed with primary specific antibodies followed by HRP conjugated antibodies (Jackson ImmunoResearch Laboratories), and developed by ECL (GE Healthcare) method, according to the manufacturer's instructions. Antibodies were: monoclonal anti-MITF (Ab-1, C5

Neomarkers), CLN (Stressgene); polyclonal rabbit anti-pCREB (phospho-CREB, Ser133, Cell Signaling), anti-pERK 1/2 (Santa Cruz), anti-TYR αPEP7, (Kobayashi et al, 1998), anti-TYRP1 αPEP1, (Kobayashi et al, 1998), anti-DCT αPEP8, (Tsukamoto et al, 1992), and anti-PMEL αPEP13, (Zhou et al, 1994) from Hearing's laboratory.

In order to compare signal intensity after αMSH and CHX treatments, band densities were quantitated with the ImageJ program, and the relative intensity of each band was normalized to the corresponding band of CLN.

**RNA isolation, cDNA synthesis and real-time quantitative RT-PCR (qPCR)**

Total RNA was extracted using TRIzol reagent (Life Technologies) or RNeasy MiniKit (Qiagen), according to the manufacturer's instructions. RNA concentration and purity were determined by measuring absorbance at 260, 230 and 280 nm; 1µg total RNA was run on a 1% agarose gel to verify RNA integrity. Starting from about 1µg of total RNA, cDNA was synthesized by using Oligo(dT)15 primers (Promega), and M-MLV Reverse Transcriptase (Promega). cDNAs were diluted 1 in 5, then subjected to qPCR analysis. The mRNA for *Mitf* was measured by Real-Time PCR (TaqMan) using the Eppendorf Mastecycler Realplex apparatus. The mouse *Mitf* primers and probe sequences were: forward 5'AGAAGCTGGAGCATGCGAAC, reverse 5'GGGAAAGTCCATGCGCTCTA and probe 5'-FAM-TGCTCAGAGTACAGGAGCTGGAGATGCAG-TAMRA-3'.

To avoid possible signal production from potential contaminating genomic DNA, specific primers and probes were designed across a common exon–intron splice junction by the Primer Express software (Applied Biosystems). For endogenous control, the expression of *Hprt* gene was examined by qPCR as described above. The sequences of primers and probe were: forward 5'TCA TTA TGC CGA GGA TTT GGA, reverse 5' ACA ATG TGA TGG CCT CCC A and probe 5'-FAM-ACAGGACTGAAAGACTTGCTCGAGATGTCATG-TAMRA-3'.

**Melanin quantification**

*Oa1*$^{+/+}$ and *Oa1*$^{-/-}$ cells were washed 2x in PBS buffer and dissolved, at the concentration of $10^6$ in 100µl, in 1 N NaOH in 10% dimethylsulfoxide, then incubated at 90°C for 30 min. After centrifugation at 1000x g for 10 min, the supernatant was taken to measure the protein concentration and melanin. The amount of melanin was measured with a spectrophotometer at 450 nm, using synthetic melanin (Sigma M-8631) as a standard, whereas the amount of proteins was analyzed by the Bio-Rad Dc Protein Assay (BioRad). Results were expressed as mean ±SD (n=7) of micrograms of melanin/milligrams of protein.

**Bright field and immunofluorescence microscopy**

For bright field and immunofluorescence microscopy, cells were grown directly on 100 $mm^2$ coverslips, fixed in 3% paraformaldehyde and permeabilized with 0.2% saponin. For MITF nuclear detection cells were fixed in methanol at –20°C for 5' followed by acetone at RT for 2 min.

Fluorochrome-conjugated secondary antibodies were from Jackson Laboratory. Samples were inspected on an Olympus inverted fluorescence microscope (model IX70). Images were recorded with a digital CCD camera (model C4742-95, Hamamatsu), using the IPLab spectrum V3.2 software package (Scanalytics) and processed with Adobe Photoshop 7.0 (Adobe Systems).

Antibodies used were: monoclonal anti-MITF (Ab-1, C5 Neomarkers), anti-PMEL (HMB45, DAKO) and a polyclonal rabbit antiserum against mouse OA1 (N45) (Cortese et al, 2005).

**Electron microscopy (EM) of flat-embedded cells**

Cell lines for EM were grown on Lab-Tek Chamber Slides™ (Nalgene Nunc International) for two days and fixed in 0.1 M cacodylate buffer containing 2.5% glutaraldehyde for 3h at room temperature. Samples were post-fixed in osmium tetroxide (EM Science) for 2h and in uranyl acetate (EM Science) for 1h at room temperature. Samples were then dehydrated through a graded ethanol series with propylene oxide as a transition fluid (TAAB Laboratories Equipment) and embedded in epoxy resin (Poly-Bed) overnight at 42°C then for 2 days at 60°C.

Ultrathin longitudinal sections of 60nm for *Oa1*$^{-/-}$ and infected cells and 250nm for *Oa1*$^{+/+}$ cells were cut and stained with uranyl acetate and lead citrate. Sections of flat-embedded cells were observed with a FEI Tecnai 12-G2 Electron Microscope (FEI Company).

The flat-embedding technique allows preservation of the original morphology of the cultured cells and permits a quantitative analysis in different areas of the cells. In order to determine the density of melanosomes in the total, central and dendritic areas, EM images were randomly taken from sections displaying both the nucleus and the dendrites. The central area was defined as the region of the cells, between the nuclear membrane and a line drawn 3,5 µm inside the plasma membrane. The dendritic area was defined by tracing the contour of dendrites from their attachment to the cell body to the tip. Melanosomes were classified according to Marks & Seabra, 2001; namely: stage II, contain unpigmented fibrillar striations; stage III, contain pigmented, electron-dense fibrillar striations; stage IV, fully pigmented organelles with non-apparent striations. Melanosome density was calculated by counting the number of melanosomes per square micron of cell profile surface. The cell area analyzed was measured by the freeshare software ImageJ (rsbweb.nih.gov/ij/) and expressed in square micrometers. Total areas of 1500, 1800, 1400 and 4000 $\mu m^2$ from at least 10 micrographs randomly acquired at 4800X, were analyzed in *Oa1*$^{+/+}$, *Oa1*$^{-/-}$, *Oa1*$^{-/-}$L*Oa1*SN, *Oa1*$^{-/-}$LSN respectively.

Stage IV melanosome diameter was considered along the major apparent axis of the organelle: at least 800 stage IV melanosomes in *Oa1*$^{-/-}$ cells, and 500 in Melan *Oa1*$^{+/+}$, *Oa1*$^{-/-}$L*Oa1*SN, *Oa1*$^{-/-}$LSN, were measured.

**Statistical analysis.**

Each plot of protein kinetics analyzed after αMSH treatment was obtained from three independent experiments. Mean and SEM were shown for each time point.

Statistical analysis of EM data was carried out using Student's unpaired t-test assuming equal variances. Data are presented as mean ± SD and were considered statistically different at $P < 0.05$. In all related panels, $P < 0.05$ is marked with single asterisk, $P < 0.01$ is labeled with double asterisks and $P<0.001$ is marked with three asterisks.

ACNOWLEDGEMENTS

We thank Dr. V.J. Hearing, for providing useful reagents; Luisa Lanfrancone, Roberto Gherzi and Tullio Florio for helpful discussions; Clara Santangelo, and Cristina Gagliani for help with electron micrographs; Tiziana Daniele for critical reading the manuscript.

This work was supported by grants from Fondazione San Paolo (2011.1172), Italian Ministry of University and Research (PRIN grant) and Italian Association for Cancer Research (AIRC IG 12035) to CT.; by Telethon-Italy (GP0443Y02 to C.V and GGP08156 to MVS); Vision of Children Foundation, San Diego, USA (to MVS). The funders had no role in study design, data collection and analysis, decision to publish, or preparation of the manuscript.

REFERENCES

Bennett DC, Cooper PJ, Hart IR (1987) A line of non-tumorigenic mouse melanocytes, syngeneic with the B16 melanoma and requiring a tumour promoter for growth. *Int J Cancer* **39:** 414-418

Bentley NJ, Eisen T, Goding CR (1994) Melanocyte-specific expression of the human tyrosinase promoter: activation by the microphthalmia gene product and role of the initiator. *Molecular and Cellular Biology* **14:** 7996-8006

Berson JF, Harper DC, Tenza D, Raposo G, Marks MS (2001) Pmel17 initiates premelanosome morphogenesis within multivesicular bodies. *Mol Biol Cell* **12:** 3451-3464

Berson JF, Theos AC, Harper DC, Tenza D, Raposo G, Marks MS (2003) Proprotein convertase cleavage liberates a fibrillogenic fragment of a resident glycoprotein to initiate melanosome biogenesis. *J Cell Biol* **161:** 521-533

Bertolotto C, Abbe P, Hemesath TJ, Bille K, Fisher DE, Ortonne JP, Ballotti R (1998) Microphthalmia gene product as a signal transducer in cAMP-induced differentiation of melanocytes. *J Cell Biol* **142:** 827-835

Carreira S, Goodall J, Aksan I, La Rocca SA, Galibert M-D, Denat L, Larue L, Goding CR (2005) Mitf cooperates with Rb1 and activates p21Cip1 expression to regulate cell cycle progression. *Nature* **433:** 764-769

Chi A, Valencia JC, Hu Z-Z, Watabe H, Yamaguchi H, Mangini NJ, Huang H, Canfield VA, Cheng KC, Yang F, Abe R, Yamagishi S, Shabanowitz J, Hearing VJ, Wu C, Appella E, Hunt DF (2006) Proteomic and bioinformatic characterization of the biogenesis and function of melanosomes. *J*

*Proteome Res* **5:** 3135-3144

Chiaverini C, Beuret L, Flori E, Busca R, Abbe P, Bille K, Bahadoran P, Ortonne JP, Bertolotto C, Ballotti R (2008) Microphthalmia-associated transcription factor regulates RAB27A gene expression and controls melanosome transport. *J Biol Chem.* **283** 12635-42

Cortese K, Giordano F, Surace EM, Venturi C, Ballabio A, Tacchetti C, Marigo V (2005) The ocular albinism type 1 (OA1) gene controls melanosome maturation and size. *Invest Ophthalmol Vis Sci* **46:** 4358-4364

Du J, Miller AJ, Widlund HR, Horstmann MA, Ramaswamy S, Fisher DE (2003) MLANA/MART1 and SILV/PMEL17/GP100 are transcriptionally regulated by MITF in melanocytes and melanoma. *Am J Pathol* **163:** 333-343

Garner A, Jay BS (1980) Macromelanosomes in X-linked ocular albinism. *Histopathology* **4:** 243-254

Giordano F, Bonetti C, Surace EM, Marigo V, Raposo G (2009) The ocular albinism type 1 (OA1) G-protein-coupled receptor functions with MART-1 at early stages of melanogenesis to control melanosome identity and composition. *Hum Mol Genet* **18:** 4530-4545

Haflidadottir BS, Bergsteinsdottir K, Praetorius C, Steingrimsson E (2010) miR-148 regulates Mitf in melanoma cells. *PloS one* **5:** e11574

Hurbain I, Geerts WJC, Boudier T, Marco S, Verkleij AJ, Marks MS, Raposo G (2008) Electron tomography of early melanosomes: implications for melanogenesis and the generation of fibrillar amyloid sheets. *Proc Natl Acad Sci USA* **105:** 19726-19731

Incerti B, Cortese K, Pizzigoni A, Surace EM, Varani S, Coppola M, Jeffery G, Seeliger M, Jaissle G, Bennett DC, Marigo V, Schiaffino MV, Tacchetti C, Ballabio A (2000) Oa1 knock-out: new insights on the pathogenesis of ocular albinism type 1. *Hum Mol Genet* **9:** 2781-2788

Innamorati G, Piccirillo R, Bagnato P, Palmisano I, Schiaffino MV (2006) The melanosomal/lysosomal protein OA1 has properties of a G protein-coupled receptor. *Pigment Cell Res* **19:** 125-135

Introne W, Boissy RE, Gahl WA (1999) Clinical, molecular, and cell biological aspects of Chediak-Higashi syndrome. *Mol Genet Metab* **68:** 283-303

Kinsella TM, Nolan GP (1996) Episomal vectors rapidly and stably produce high-titer recombinant retrovirus. *Hum Gene Ther* **7:** 1405-1413

Kobayashi T, Imokawa G, Bennett DC, Hearing VJ (1998) Tyrosinase stabilization by Tyrp1 (the brown locus protein). *J Biol Chem* **273:** 31801-31805

Kobayashi T, Urabe K, Orlow SJ, Higashi K, Imokawa G, Kwon BS, Potterf B, Hearing VJ (1994) The Pmel 17/silver locus protein. Characterization and investigation of its melanogenic function. *J Biol Chem* **269:** 29198-29205

Marks MS, Heijnen HF, Raposo G (2013) Lysosome-related organelles: unusual compartments become mainstream. *Curr Opin Cell Biol.* **4:** 495-505

Marks MS, Seabra MC (2001) The melanosome: membrane dynamics in black and white. *Nat Rev Mol Cell Biol* **2:** 738-748

McGlinchey RP, Shewmaker F, McPhie P, Monterroso B, Thurber K, Wickner RB (2009) The repeat

domain of the melanosome fibril protein Pmel17 forms the amyloid core promoting melanin synthesis. *Proceedings of the National Academy of Sciences of the United States of America* **106:** 13731-13736

Miller AD, Rosman GJ (1989) Improved retroviral vectors for gene transfer and expression. *BioTechniques* **7:** 980-982, 984-986, 989-990

Morgenstern JP, Land H (1990) Advanced mammalian gene transfer: high titre retroviral vectors with multiple drug selection markers and a complementary helper-free packaging cell line. *Nucleic acids research* **18:** 3587-3596

Newton RA, Cook AL, Roberts DW, Leonard JH, Sturm RA (2007) Post-transcriptional regulation of melanin biosynthetic enzymes by cAMP and resveratrol in human melanocytes. *J Invest Dermatol* **127:** 2216-2227

O'Donnell FE, Hambrick GW, Green WR, Iliff WJ, Stone DL (1976) X-linked ocular albinism. An oculocutaneous macromelanosomal disorder. *Arch Ophthalmol* **94:** 1883-1892

Palmisano I, Bagnato P, Palmigiano A, Innamorati G, Rotondo G, Altimare D, Venturi C, Sviderskaya EV, Piccirillo R, Coppola M, Marigo V, Incerti B, Ballabio A, Surace EM, Tacchetti C, Bennett DC, Schiaffino MV (2008) The ocular albinism type 1 protein, an intracellular G protein-coupled receptor, regulates melanosome transport in pigment cells. *Hum Mol Genet* **17:** 3487-3501

Price ER, Horstmann MA, Wells AG, Weilbaecher KN, Takemoto CM, Landis MW, Fisher DE (1998) alpha-Melanocyte-stimulating hormone signaling regulates expression of microphthalmia, a gene deficient in Waardenburg syndrome. *J Biol Chem* **273:** 33042-33047

Proudfoot NJ, Furger A, Dye MJ (2002) Integrating mRNA processing with transcription. *Cell* **108:** 501-512

Saeki H, Oikawa A (1980) Synthesis and degradation of tyrosinase in cultured melanoma cells. *Journal of cellular physiology* **104:** 171-175

Samaraweera P, Shen B, Newton JM, Barsh GS, Orlow SJ (2001) The mouse ocular albinism 1 gene product is an endolysosomal protein. *Exp Eye Res* **72:** 319-329

Schiaffino MV (2010) Signaling pathways in melanosome biogenesis and pathology. *Int J Biochem Cell Biol* **42:** 1094-1104

Schiaffino MV, d'Addio M, Alloni A, Baschirotto C, Valetti C, Cortese K, Puri C, Bassi MT, Colla C, De Luca M, Tacchetti C, Ballabio A (1999) Ocular albinism: evidence for a defect in an intracellular signal transduction system. *Nat Genet* **23:** 108-112

Schiaffino MV, Dellambra E, Cortese K, Baschirotto C, Bondanza S, Clementi M, Nucci P, Ballabio A, Tacchetti C, De Luca M (2002) Effective retrovirus-mediated gene transfer in normal and mutant human melanocytes. *Hum Gene Ther* **13:** 947-957

Settembre C, Zoncu R, Medina DL, Vetrini F, Erdin S, Huynh T, Ferron M, Karsenty G, Vellard MC, Facchinetti V, Sabatini DM, Ballabio A (2012) A lysosome-to-nucleus signalling mechanism senses and regulates the lysosome via mTOR and TFEB. *The EMBO journal* **31:** 1095-1108

Shen B, Rosenberg B, Orlow SJ (2001) Intracellular distribution and late endosomal effects of the ocular albinism type 1 gene product: consequences of disease-causing mutations and implications for melanosome biogenesis. *Traffic* **2:** 202-211

Solano F, Martínez-Esparza M, Jiménez-Cervantes C, Hill SP, Lozano JA, García-Borrón JC (2000) New insights on the structure of the mouse silver locus and on the function of the silver protein. *Pigment Cell Res* **13 Suppl 8:** 118-124

Staleva L, Orlow SJ (2006) Ocular albinism 1 protein: trafficking and function when expressed in Saccharomyces cerevisiae. *Exp Eye Res* **82:** 311-318

Steingrímsson E, Copeland NG, Jenkins NA (2004) Melanocytes and the microphthalmia transcription factor network. *Annu Rev Genet* **38:** 365-411

Theos AC, Berson JF, Theos SC, Herman KE, Harper DC, Tenza D, Sviderskaya EV, Lamoreux ML, Bennett DC, Raposo G, Marks MS (2006a) Dual loss of ER export and endocytic signals with altered melanosome morphology in the silver mutation of Pmel17. *Mol Biol Cell* **17:** 3598-3612

Theos AC, Truschel ST, Tenza D, Hurbain I, Harper DC, Berson JF, Thomas PC, Raposo G, Marks MS (2006b) A lumenal domain-dependent pathway for sorting to intralumenal vesicles of multivesicular endosomes involved in organelle morphogenesis. *Dev Cell* **10:** 343-354

Tsukamoto K, Jackson IJ, Urabe K, Montague PM, Hearing VJ (1992) A second tyrosinase-related protein, TRP-2, is a melanogenic enzyme termed DOPAchrome tautomerase. *EMBO J* **11:** 519-526

Vachtenheim J, Borovanský J (2010) "Transcription physiology" of pigment formation in melanocytes: central role of MITF. *Exp Dermatol* **19:** 617-627

van de Wetering M, Oving I, Muncan V, Pon Fong MT, Brantjes H, van Leenen D, Holstege FCP, Brummelkamp TR, Agami R, Clevers H (2003) Specific inhibition of gene expression using a stably integrated, inducible small-interfering-RNA vector. *EMBO Rep* **4:** 609-615

Vetrini F, Tammaro R, Bondanza S, Surace EM, Auricchio A, De Luca M, Ballabio A, Marigo V (2006) Aberrant splicing in the ocular albinism type 1 gene (OA1/GPR143) is corrected in vitro by morpholino antisense oligonucleotides. *Hum Mutat* **27:** 420-426

Watt B, Tenza D, Lemmon MA, Kerje S, Raposo G, Andersson L, Marks MS (2011) Mutations in or near the transmembrane domain alter PMEL amyloid formation from functional to pathogenic. *PLoS genetics* **7:** e1002286

Watt B, van Niel G, Fowler DM, Hurbain I, Luk KC, Stayrook SE, Lemmon MA, Raposo G, Shorter J, Kelly JW, Marks MS (2009) N-terminal domains elicit formation of functional Pmel17 amyloid fibrils. *The Journal of biological chemistry* **284:** 35543-35555

Young A, Jiang M, Wang Y, Ahmedli NB, Ramirez J, Reese BE, Birnbaumer L, Farber DB (2011) Specific interaction of Galphai3 with the Oa1 G-protein coupled receptor controls the size and density of melanosomes in retinal pigment epithelium. *PloS one* **6:** e24376

Zhou BK, Kobayashi T, Donatien PD, Bennett DC, Hearing VJ, Orlow SJ (1994) Identification of a melanosomal matrix protein encoded by the murine si (silver) locus using "organelle scanning". *Proc Natl Acad Sci U S A* **91:** 7076-7080

FIGURE LEGENDS

**Figure 1. Absence of OA1 affects melanocyte shape and melanosome number, size and maturation.** EM images (A-D) and bright field optical pictures (inset A' and B'). (A-B) *Oa1*$^{+/+}$ cells

display lack of dendrites, and an almost homogeneous distribution and size of mature melanosomes. *Oa1*$^{-/-}$ cells exhibit a dendritic shape with long, thin dendrites rich of mature melanosomes, and a central region depleted of mature and immature stages Bars: 10 µm. (C-D) in *Oa1*$^{+/+}$ cells the peripheral area is full of mature as well as immature melanosomes, whereas the dendrites of *Oa1*$^{-/-}$ cells are deficient in immature melanosomes. Both normal and giant melanosomes are found in OA1-deficient melanocytes. Bars: 1µm. (E) Quantification of the maturation stages of melanosomes in *Oa1*$^{+/+}$ and *Oa1*$^{-/-}$ cells. Results are presented as density of different stages of maturation (melanosomes/µm$^2$). *Oa1*$^{-/-}$ cells show a sizable decrease of all the maturation stages and a halving of mature organelles. Melanosomes were counted on randomly acquired micrographs at 16500X magnification for *Oa1*$^{+/+}$ (n= 1074 melanosomes; total area= 505 µm$^2$; micrographs= 27) and *Oa1*$^{-/-}$ cells (n= 1278 melanosomes; total area= 1830 µm$^2$, micrographs=51). ***P<0.001 (independent samples Student's *t*-test assuming equal variances). (F) Analysis of melanosomal size. Histograms represent the percent in size of measured melanosomes. *Oa1*$^{+/+}$ cells display melanosomes with a homogeneous size (NORMAL). Differently, *Oa1*$^{-/-}$ melanosomes have a significant variability in size: just 35% of melanosomes are comparable in size with the *wild-type* melanosomes, more than 60% of melanosomes altogether show an aberrant dimension: ENLARGED melanosomes are more than 40% and MACRO melanosomes are about 20%. n=400 and n=800 melanosomes were measured in 5 different profiles for *Oa1*$^{+/+}$ and *Oa1*$^{-/-}$ respectively. (G) Melanin quantification: *Oa1*$^{+/+}$ and *Oa1*$^{-/-}$ protein extracts reveal the same melanin content. Values are represented as mean ±SD (n=7) of micrograms of melanin/milligrams of protein.

**Figure 2. *Oa1* transduction in *Oa1*$^{-/-}$ cells rescues number and size of melanosomes.**

(A) Immunofluorescence picture representing OA1 expression and endo-lysosomal distribution pattern in *Oa1*$^{-/-}$L*Oa1*SN cells**.** Bar: 20 µm. (B) Flat-embedded *Oa1*$^{-/-}$LSN; note the complete absence of immature melanosomes in the central area. Bar: 0.5 µm. (C) Central area of *Oa1*$^{-/-}$L*Oa1*SN cells showing an abundant accumulation of stage II and stage III melanosomes. Bar: 1 µm. (D-F) Quantification of the maturation stages of melanosomes presented as density (melanosomes/µm$^2$). (D) In the total area, significant increase of stage II melanosomes was observed in *Oa1*$^{-/-}$L*Oa1*SN in comparison to *Oa1*$^{-/-}$LSN. *P<0.05 (P=0.031). *Oa1*$^{-/-}$L*Oa1*SN: n= 2768 melanosomes; total area= 3950 µm$^2$, micrographs=23; *Oa1*$^{-/-}$LSN: n= 1980 melanosomes; total area= 2800 µm$^2$, micrographs=16. (E) In central area *Oa1*$^{-/-}$L*Oa1*SN cells show a sizable increase of stage II (10-fold) and stage III (5-fold) melanosomes in comparison to *Oa1*$^{-/-}$LSN. Melanosomes were counted in the central area (defined in Matherials and Methods, EM section), on randomly acquired micrographs at 4800X magnification for *Oa1*$^{-/-}$L*Oa1*SN (n= 939; total area= 1080 µm$^2$; micrographs= 10) and *Oa1*$^{-/-}$ LSN cells (n= 321; total area= 1130 µm$^2$, micrographs=9). **P<0.01; ***P<0.001 (independent samples Student's *t*-test assuming equal variances.). (F) In dendritic area of both cell lines no significant variations in all stage melanosomes were observed; *Oa1*$^{-/-}$L*Oa1*SN: n= 709 melanosomes;

total area= 660 µm$^2$, micrographs=7; *Oa1*$^{-/-}$LSN: n= 270; total area= 270 µm$^2$, micrographs=6. (G) Histograms represent the frequency of melanosomes size measured in at least 500 melanosomes in 5 different cells for each cell line. Histograms show a decrease in size of both ENLARGED and MACRO melanosomes after *Oa1* transduction. Analyses were preformed two months post-infection.

**Figure 3. OA1 expression affects melanosomal proteins.** (A) Blots of total protein extracts were probed with antibodies against the melanin synthesis enzyme PEP7 (TYR) and structural protein PEP13 (PMEL). CLN was used as loading control. While levels of TYR were not affected by *Oa1* absence, both *Oa1*$^{-/-}$ and shOA1 show a sizable decrease in both the P1 and Mß processed forms of PMEL protein levels. (B) Quantification of the protein amount in A, expressed as fold change relative to *Oa1*$^{+/+}$ cells. (C) Measured mRNA levels by qPCR show 55% of reduction fo*r Pmel* and 45% for *Tyr* in *knock-out* cells, compared to controls. Results are presented as mean ± SD of 3 independent experiments.

**Figure 4. MITF protein and mRNA levels are influenced by the presence of OA1**. Absence of OA1 determines a reduction in MITF levels when analyzed by Western Blot, Immunofluorescence and qPCR in cells *knock-out* and silenced for *Oa1*, in comparison to their relative controls. (A) Both phosphorylated, upper band, and basal MITF forms are strongly reduced in *Oa1*$^{-/-}$ and shOA1. (B) Nuclear staining for MITF show a decrease in cells depleted for OA1. Bars: 10 µm. (C) OA1 absence does not influence MITF protein degradation. *Oa1*$^{+/+}$ versus *Oa1*$^{-/-}$ and shCTR versus shOA1 treated with CHX for the indicated times. Both the OA1-depleted cells, compared to proper controls, show a comparable degradation rate and protein half-life. Densitometric analysis expressed as mean ± SD, n=3. (D) *Mitf* mRNA levels were measured by qPCR and show 45% (n=4) and 55% (n=3) of reduction for *knock-out* and shOA1 cells, respectively. Data are represented as mean ± SD.

**Figure 5. Re-expression of OA1 or MITF is capable to restore PMEL.** (A) OA1 re-expression restores MITF: Western Blot analysis shows a rescue quantified as about two-fold increase, for both basal and phosphorylated MITF protein in comparison to the *Oa1*$^{-/-}$LSN control cells (n=4). (B) OA1 re-expression partially restores the PMEL protein levels in *Oa1*$^{-/-}$L*Oa1*SN cells 14 days after transduction. Of note, the biochemical rescue of PMEL is partial, but only 50% of these cells are effectively expressing OA1. (C) MITF re-expression efficiently restores the PMEL protein levels in *Oa1*$^{-/-}$ pBabe-*Mitf* after 7 days of transduction. (D) Representative immunofluorescence pictures of OA1 and PMEL stained with HMB45 antibody. On the left, *Oa1*$^{-/-}$ cells show few and scattered HMB45 positive structures; on the right, double immunofluorescence assay showing OA1 and PMEL expression in *Oa1*$^{-/-}$L*Oa1*SN cells. Note the increased PMEL staining in cells re-expressing OA1. Bars: 5 µm.

**Figure 6. OA1 sustains the MITF levels via αMSH pathway.** (A-B) *Oa1*$^{+/+}$ and *Oa1*$^{-/-}$ cells, and (C) shOA1 and shCTR were treated with 1 μM αMSH for the indicated times. Total lysates were probed for MITF. *Oa1*$^{+/+}$ cells and shCTR show an increase in MITF amount, maintained along the treatment, while *Oa1*$^{-/-}$ and shOA1 cells are unable to sustain MITF levels beyond 3h of treatment. To note: double amount of cell extracts have been loaded for *Oa1*$^{-/-}$compared to control cells, to better visualize and quantify bands intensity. (B) Protein quantification. *Oa1*$^{+/+}$ cells responded to αMSH stimulus with a 2.5 times fold increase of MITF protein amount at 3h of treatment. This increase is sustained beyond, in line with previous studies on normal human melanocytes (Newton et al, 2007). At steady state, *Oa1*$^{-/-}$ differs from *Oa1*$^{+/+}$ showing a reduced amount of MITF protein quantified as about 50% less. Despite this reduced amount, after 3h of αMSH treatment *Oa1*$^{-/-}$ were able to reach the same amount of MITF as *wild-type* cells, increasing their absolute fold increase about 5 times and demonstrating a correct responsiveness to αMSH stimulation. Even so, *Oa1*$^{-/-}$ showed a rapid decrease of MITF protein levels between 3 and 6h and successive point of analysis. Values represent the mean ±SD (n=3) and are expressed as Fold Increase compared to the untreated *wild-type* cells. (D) Protein degradation is not responsible for MITF decrease in *Oa1*$^{-/-}$ melanocytes. Cells were stimulated with 1μM αMSH for 6h. After 3h of stimulation half of the cells were treated with 100μg/ml CHX and harvested after additional 1, 2 and 3h. *Oa1*$^{+/+}$ show a decrease of MITF protein levels after CHX treatment. On the contrary MITF amount in *Oa1*$^{-/-}$ cells was not influenced by the presence of the drug. Values on the chart represent the mean ±SD, (n=3).

**Figure 7. OA1 does not influence *Mitf* mRNA degradation and regulates *Mitf* transcription.** qPCR of *Mitf* mRNA in presence of αMSH and/or Actinomycin D (ActD). (A) *Oa1*$^{+/+}$ and *Oa1*$^{-/-}$ cells were treated with αMSH 1μM in a time course of 5h, then analyzed to visualize *Mitf* mRNA modulation. Note that while *Mitf* levels in *Oa1*$^{+/+}$ cells increase during αMSH stimulation, in *Oa1*$^{-/-}$ cells decrease after 1h of treatment. Values are expressed as *Mitf* Fold Increase compared to the untreated *wild-type* cells. (B-C) mRNA degradation is not responsible for *Mitf* decrease in *Oa1*$^{-/-}$ cells. *Oa1*$^{+/+}$ and *Oa1*$^{-/-}$ cells were stimulated with 1μM αMSH for 5h. At 2h of stimulation, half of the cells were treated with 5μg/ml ActD and harvested after additional 1, 2 and 3h. Cells were analyzed by qPCR to visualize modulation of *Mitf* levels in presence of ActD in comparison to the untreated cells. Of note, while in *Oa1*$^{+/+}$ cells ActD determines a rapid decrease of *Mitf* mRNA (panel B), *Oa1*$^{-/-}$ cells (panel C) are not affected by such treatment. The kinetics are representative of n≥3 experiments. (D) *Mitf* mRNA is unstable in *Oa1*$^{+/+}$ cells but not in *Oa1*$^{-/-}$ cells at steady state condition. Exponentially growing cells were treated with 5μg/ml ActD, harvested and analyzed at indicated times. *Mitf* mRNA is rapidly degraded in presence of OA1 and is highly stable in its absence. Values are represented as mean ±SD (n=2).

**Figure 8. Model of macromelanosome formation in Oa1 depleted cells.** The presence of OA1(upper panel) sustains *Mitf* transcription via a signalling cascade cAMP-mediated. MITF regulates melanosome biogenesis leading to the transcription of PMEL, and melanin synthesis activating melanin producing enzymes, such as Tyrosinase, that will be equally distributed among the newly formed melanosomes and produce melanin. The coordinate regulation of these processes leads to the maturation of the melanosome (upper right electromicrograph).

The absence of OA1(lower panel) leads to a reduction of MITF protein amount, which determines a decrease in PMEL, and in turn a reduction of stage II melanosomes, while the amount of melanogenesis enzymes remains unaffected. Therefore, the enzymes will accumulate in the few stage II melanosomes available, determining excess in melanin production eventually leading to macromelanosome. The lower right micrograph shows macromelanosomes with a fibrillar central core of the size of a normal melanosome.

SUPPLEMENTARY FIGURE LEGENDS

**Figure S1. The actin cytoskeleton and Rab27a are not affected by OA1 depletion.** (A) Representative immunofluorescence pictures stained with phalloidin show the very similar actin cytoskeleton of $Oa1^{+/+}$ and $Oa1^{-/-}$ cells (B) *Rab27a* mRNA levels were measured by qPCR and results comparable in amount in $Oa1^{+/+}$ cells and $Oa1^{-/-}$ cells.

**Figure S2. Generation of the shOA1 cell line by RNAi.** $Oa1^{+/-}$cells were stably transfected either with empty vector (shCTR) or expressing shRNA1, directed against the *Oa1* transcript (shOA1). (A) An example of semiquantitative PCR results, obtained by simultaneously amplifying the cDNAs of the indicated cell lines with primers for the *Oa1* transcript or βactin. Samples were collected at four time points during the amplification (I-IV, see Materials and Methods). *Oa1* amplification products from shOA1 cells are barely visible at cycles III-IV. (B) Quantification of *Oa1* expression in the indicated cell lines, obtained by using βactin expression for normalization. Results represent the mean ± SD (n=6) and are expressed as percent of *Oa1* amount in shCTR cells. *P <0.01, compared to shCTR, and <0.05, compared to $Oa1^{+/-}$ (paired Student's t-test assuming equal variances). (C) Representative bright field optical pictures of shCTR and shOA1 cell lines. In shOA1 cells, melanosomes appear larger (see inset for 3x magnification) and peripherally distributed, similarly to $Oa1^{-/-}$ melanocytes. Bars, 15 µm.

**Figure S3. MART1 protein levels and distribution are not affected by OA1 depletion.** (A) The IF analysis in Melan $Oa1^{-/-}$ Melan shOa1 and relative controls, shows that the presence of OA1 doesn't affect either the amount or the distribution of the protein MART1. Of note, HMB45 staining of the

different cell lines, used as a marker for stage II melanosomes, shows a disperse and less abundant pattern in cells depleted of OA1, in comparison to their relative controls. (B) Blots of total protein extracts were probed with antibody against MART1. All the models of depletion and restoration of OA1 and MITF show no changes in MART1 protein amount.

Figure 1

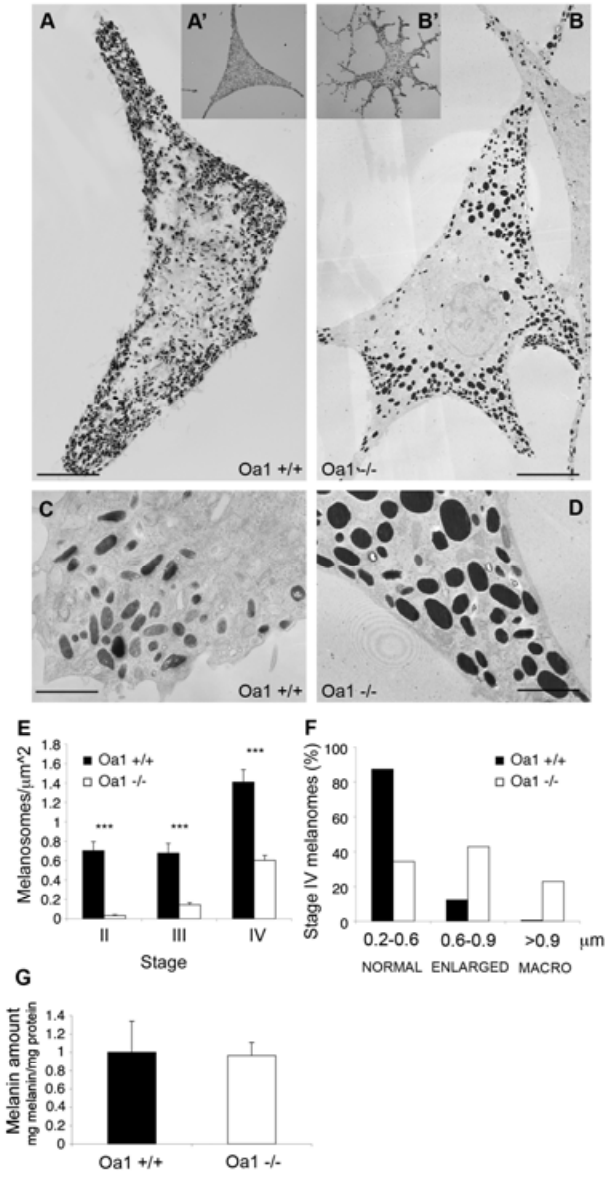

Figure 2

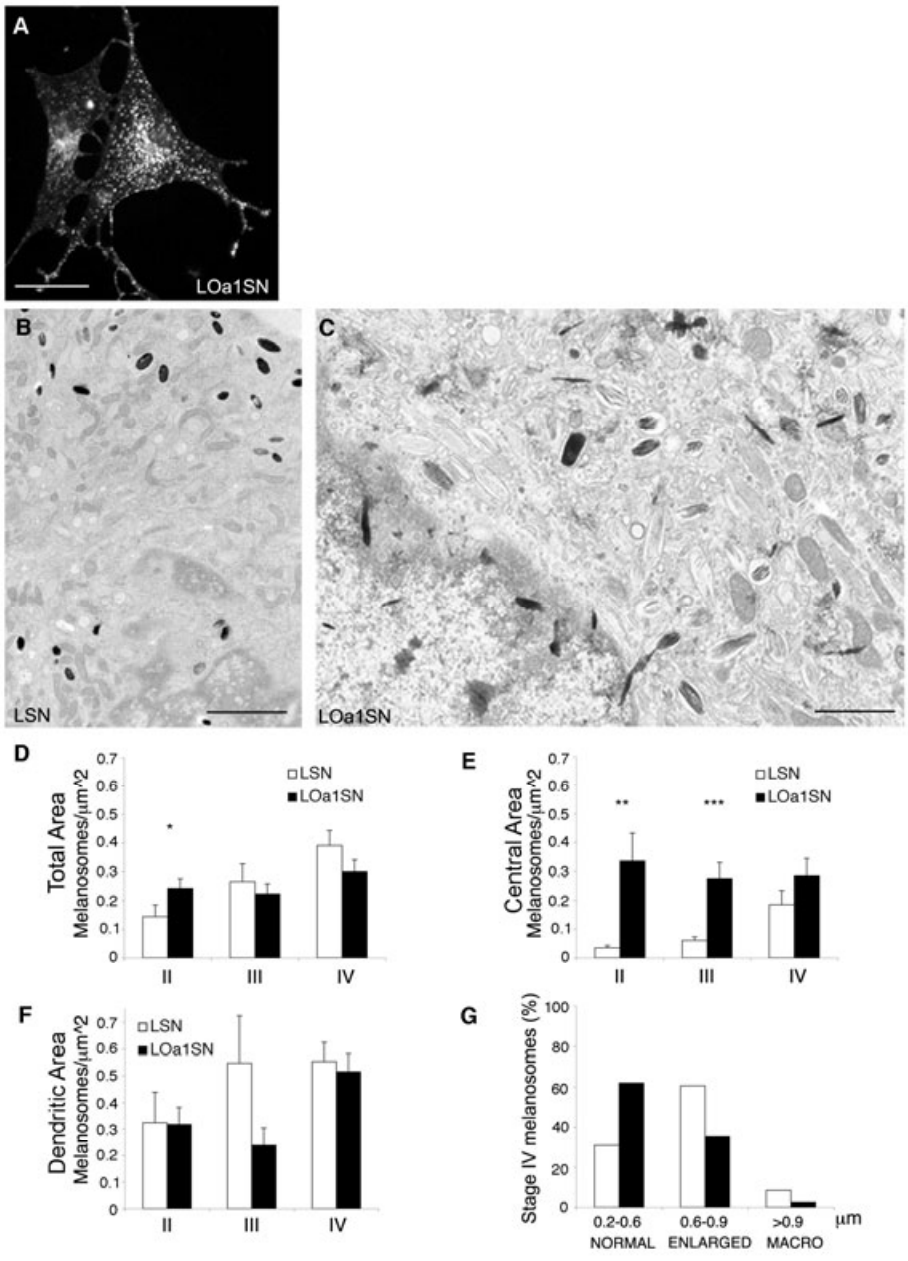

Figure 3

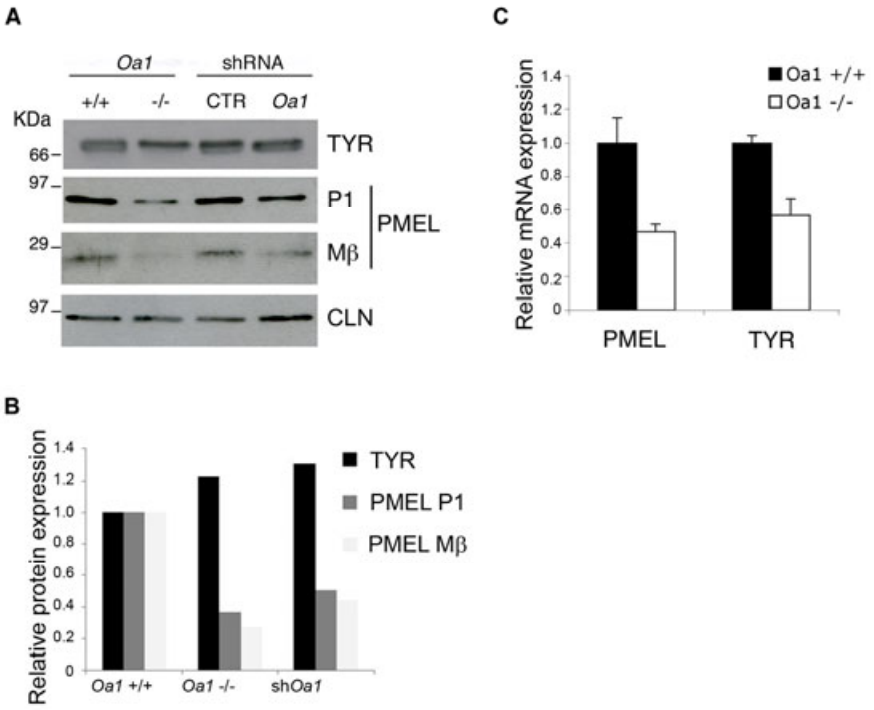

Figure 4

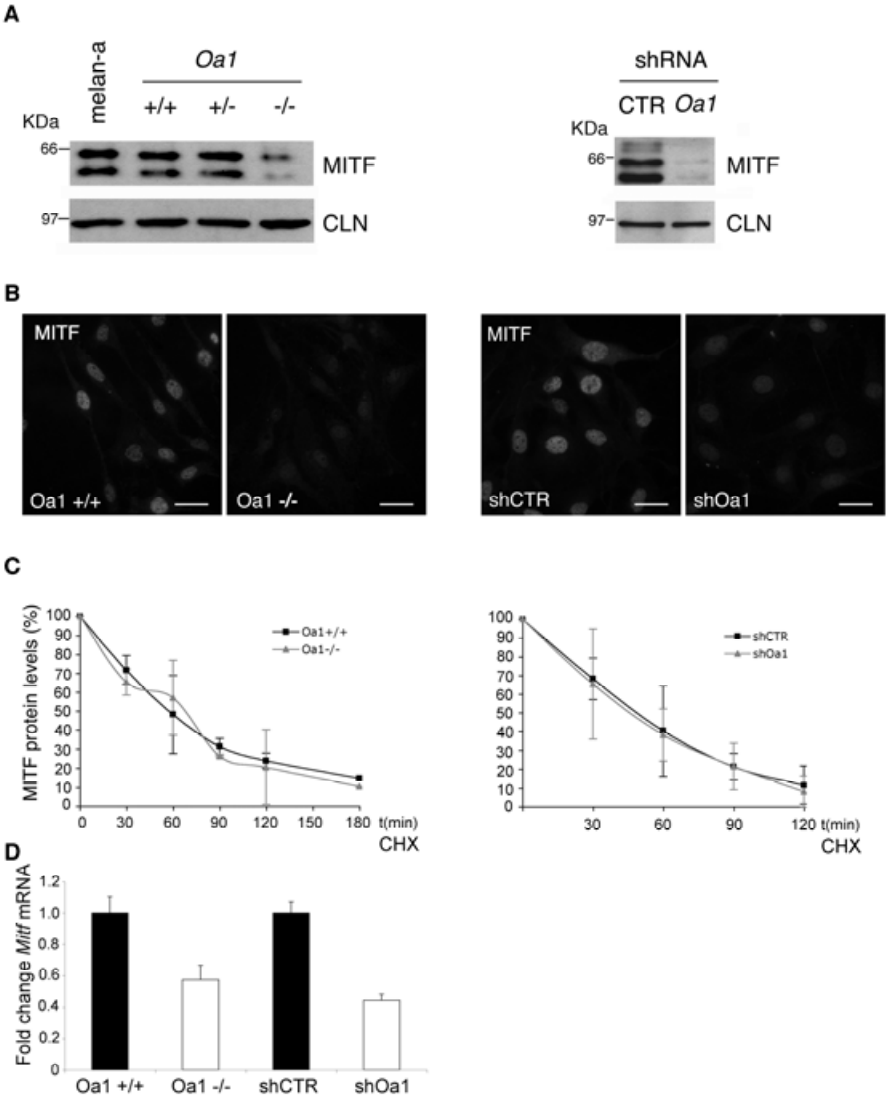

Figure 5

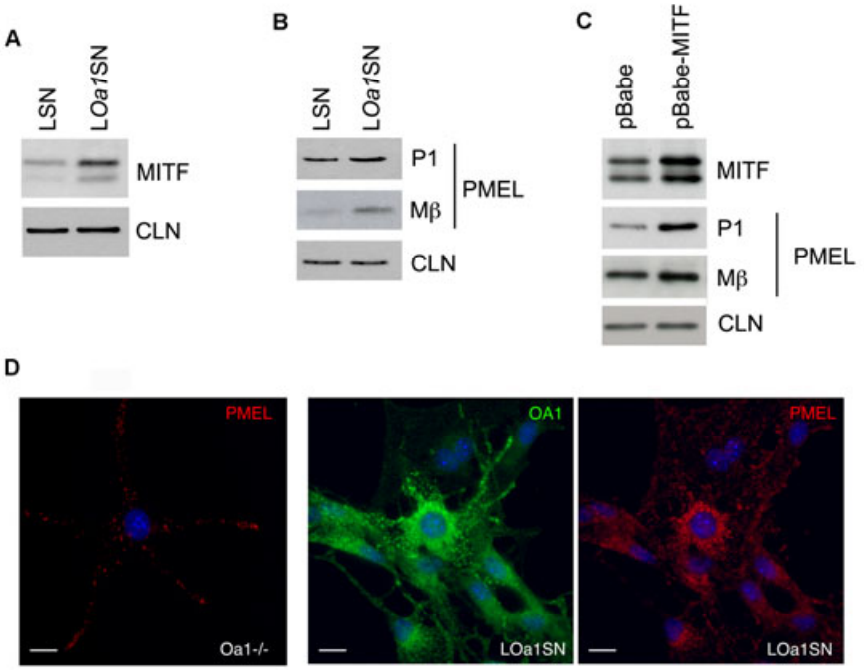

Figure 6

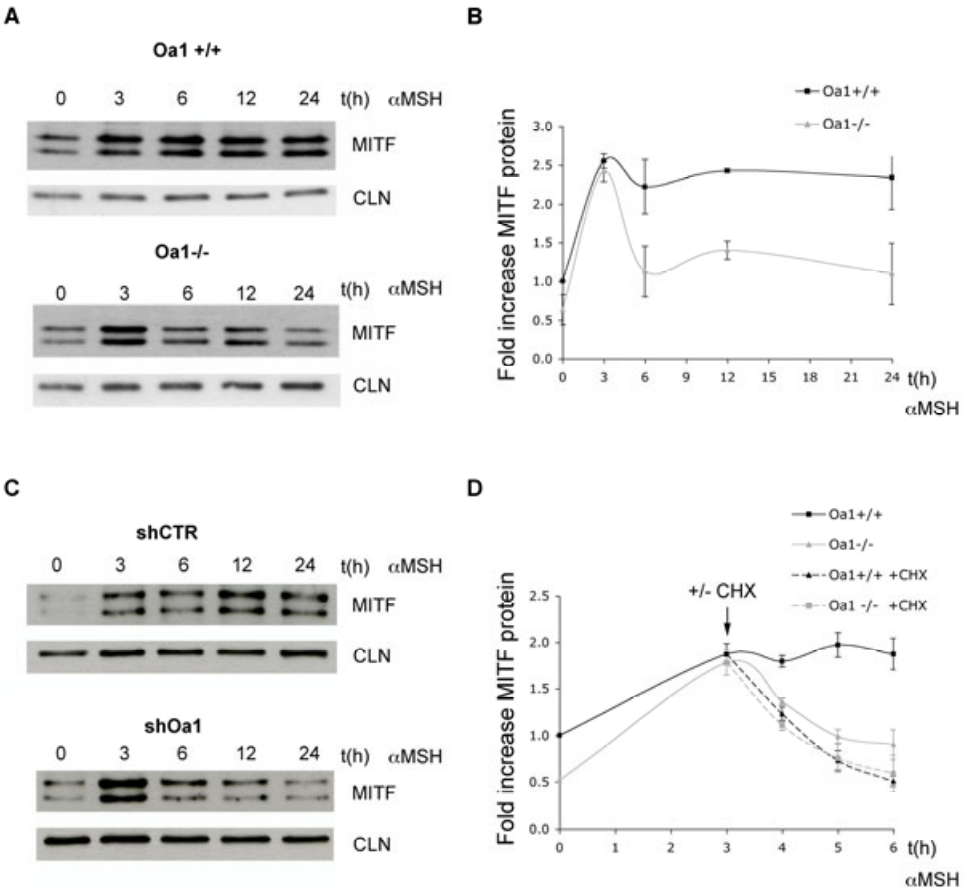

Figure 7

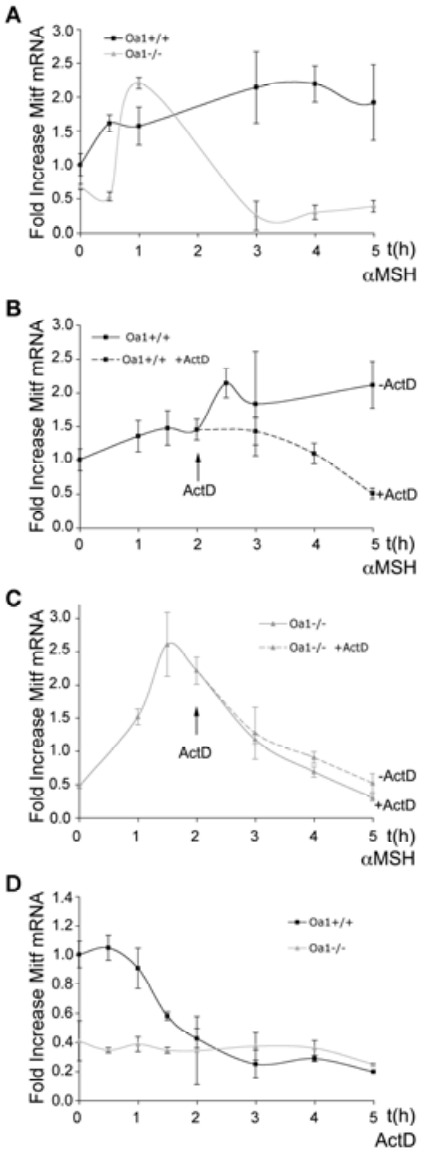

Figure 8